A method for avoiding the acoustic time-step restriction in compressible flow

Nipun Kwatra * Jonathan Su * Jón T. Grétarsson *
Ronald Fedkiw **

Stanford University, 353 Serra Mall Room 207, Stanford, CA 94305

Abstract

We propose a novel method for alleviating the stringent CFL condition imposed by the sound speed in simulating inviscid compressible flow with shocks, contacts and rarefactions. Our method is based on the pressure evolution equation, so it works for arbitrary equations of state, chemical species etc, and is derived in a straightforward manner. Similar methods have been proposed in the literature, but the equations they are based on and the details of the methods differ significantly. Notably our method leads to a standard Poisson equation similar to what one would solve for incompressible flow, but has an identity term more similar to a diffusion equation. In the limit as the sound speed goes to infinity, one obtains the Poisson equation for incompressible flow. This makes the method suitable for two-way coupling between compressible and incompressible flows and fully implicit solid-fluid coupling, although both of these applications are left to future work. We present a number of examples to illustrate the quality and behavior of the method in both one and two spatial dimensions, and show that for a low Mach number test case we can use a CFL number of 300 (whereas previous work was only able to use a CFL number of 3 on the same example).

1 Introduction

In this paper, we focus on highly nonlinear compressible flows with shocks, contacts and rarefactions, for example the Sod shock tube. Traditionally these types of problems are solved with explicit time integration (for example Runga-Kutta methods, ENO, WENO etc, see e.g. [10,11,5]). Although these methods produce high quality results, small time steps are required in order to enforce

* {kwatra,jonsu,jontg}@stanford.edu, Stanford University
**{fedkiw}@cs.stanford.edu, Stanford University

Report Documentation Page

Form Approved
OMB No. 0704-0188

1. REPORT DATE	2. REPORT TYPE	3. DATES COVERED
28 AUG 2008		**00-00-2008 to 00-00-2008**

4. TITLE AND SUBTITLE	5a. CONTRACT NUMBER
A method for avoiding the acoustic time-step restriction in compressible flow	5b. GRANT NUMBER
	5c. PROGRAM ELEMENT NUMBER
6. AUTHOR(S)	5d. PROJECT NUMBER
	5e. TASK NUMBER
	5f. WORK UNIT NUMBER
7. PERFORMING ORGANIZATION NAME(S) AND ADDRESS(ES) **Stanford University,353 Serra Mall Room 207,Stanford,CA,94305**	8. PERFORMING ORGANIZATION REPORT NUMBER
9. SPONSORING/MONITORING AGENCY NAME(S) AND ADDRESS(ES)	10. SPONSOR/MONITOR'S ACRONYM(S)
	11. SPONSOR/MONITOR'S REPORT NUMBER(S)

12. DISTRIBUTION/AVAILABILITY STATEMENT
Approved for public release; distribution unlimited

13. SUPPLEMENTARY NOTES

14. ABSTRACT

We propose a novel method for alleviating the stringent CFL condition imposed by the sound speed in simulating inviscid compressible flow with shocks, contacts and rarefactions. Our method is based on the pressure evolution equation, so it works for arbitrary equations of state, chemical species etc, and is derived in a straightforward manner. Similar methods have been proposed in the literature, but the equations they are based on and the details of the methods differ significantly. Notably our method leads to a standard Poisson equation similar to what one would solve for incompressible flow, but has an identity term more similar to a diffusion equation. In the limit as the sound speed goes to infinity, one obtains the Poisson equation for incompressible flow. This makes the method suitable for two-way coupling between compressible and incompressible flows and fully implicit solid-fluid coupling, although both of these applications are left to future work. We present a number of examples to illustrate the quality and behavior of the method in both one and two spatial dimensions, and show that for a low Mach number test case we can use a CFL number of 300 (whereas previous work was only able to use a CFL number of 3 on the same example).

15. SUBJECT TERMS

16. SECURITY CLASSIFICATION OF:			17. LIMITATION OF ABSTRACT	18. NUMBER OF PAGES	19a. NAME OF RESPONSIBLE PERSON
a. REPORT **unclassified**	b. ABSTRACT **unclassified**	c. THIS PAGE **unclassified**	**Same as Report (SAR)**	**23**	

the CFL condition of information moving only one grid cell per time step. While this is understandable for very high Mach number flow where $|u|$, $|u-c|$ and $|u+c|$ are all of similar magnitude, it is too restrictive for flows where c may be much larger than $|u|$. Moreover some flow fields might have both high Mach number regions where shock waves are of interest as well as low Mach number regions where the material velocities are important. In this case, a large number of time steps are required if one is interested in the motion of the fluid particles over an appreciable distance in the low Mach number regions. Thus, it can be quite useful to have methods that avoid the stringent CFL time step restriction imposed by the acoustic waves and instead use only the material velocity CFL restriction (albeit one would expect some loss of quality because of the implicit treatment of the acoustic waves).

To alleviate the stringent CFL restriction, [6] proposed both a non-conservative and a conservative scheme. Their non-conservative scheme builds on the predictor-corrector type scheme of [16] to derive an elliptic pressure equation quite similar to ours, but for an adiabatic fluid. Our method is similar in spirit to [6,13–15] where we divide the calculation into two parts: advection and non-advection. The advection terms are treated with explicit time integration, and thus the CFL restriction on the material velocity remains. Whereas one can use a standard method such as ENO in solving the advection terms, we found that when coupled to an implicit solution of the pressure equations (that is inherently central-differenced) the standard ENO method sometimes leads to spurious oscillatory behavior. Thus we designed a new ENO method geared towards a MAC grid discretization of the data, making it more similar to incompressible flow. We call this MAC-ENO or MENO. The remaining non-advection terms are solved using an implicit equation for the pressure using a standard MAC grid type formulation. Since the MAC grid is dual in both velocity and pressure (noting that the MAC grid pressure needs to live at cell faces for flux based methods), one needs to interpolate data back and forth.

We base the derivation of our method on the pressure evolution equation as discussed in [2], thus making it valid for general equations of state, arbitrary chemical species etc. Thus, our derivation has less assumptions and is a bit more straight forward than previous work, especially that based on preconditioners. Also, our method is fully conservative and thus shocks are tracked at the right speed. We present a number of traditional examples for highly non-linear compressible flows including the Sod shock tube, interacting blast waves, and two dimensional flow past a step. We also demonstrate that the method works well for low Mach number flow, taking the example of [7] where the authors obtain reasonable results with a CFL number of 3. Notably, our method allows a CFL number of 300 (two orders of magnitude more).

2 Numerical Method

Let us consider the one dimensional Euler equations,

$$\begin{pmatrix} \rho \\ \rho u \\ E \end{pmatrix}_t + \begin{pmatrix} \rho u \\ \rho u^2 + p \\ Eu + pu \end{pmatrix}_x = 0$$

with ρ being the density, u the velocity, E the total energy and p the pressure. The flux term can be separated into an advection part and a non-advection part,

$$\mathbf{F_1}(\mathbf{U}) = \begin{pmatrix} \rho u \\ \rho u^2 \\ Eu \end{pmatrix}, \mathbf{F_2}(\mathbf{U}) = \begin{pmatrix} 0 \\ p \\ pu \end{pmatrix}. \tag{1}$$

We first compute the advection part with Jacobian

$$\mathbf{J} = \begin{pmatrix} 0 & 1 & 0 \\ -u^2 & 2u & 0 \\ -\frac{Eu}{\rho} & \frac{E}{\rho} & u \end{pmatrix}.$$

All the Jacobian's eigenvalues are equal to u, and it is rank deficient with left eigenvectors of $(u, -1, 0)$ and $(E/\rho, 0, -1)$ and right eigenvectors of $(1, u, 0)^T$ and $(0, 0, 1)^T$. Since all the characteristic velocities are identical, we can apply component wise upwinding to $\mathbf{F_1}(\mathbf{U})$ without having to transform into the characteristic variables first (as in [4]). Moreover, this advection part only requires a time step restriction based on u.

2.1 Implicit Pressure Update

The multi-dimensional Euler equations are

$$\begin{pmatrix} \rho \\ \rho u \\ \rho v \\ \rho w \\ E \end{pmatrix}_t + \begin{pmatrix} \rho u \\ \rho u^2 \\ \rho uv \\ \rho uw \\ Eu \end{pmatrix}_x + \begin{pmatrix} \rho v \\ \rho uv \\ \rho v^2 \\ \rho vw \\ Ev \end{pmatrix}_y + \begin{pmatrix} \rho w \\ \rho uw \\ \rho vw \\ \rho w^2 \\ Ew \end{pmatrix}_z + \begin{pmatrix} 0 \\ \nabla p \\ \nabla \cdot (p\vec{u}) \end{pmatrix} = 0.$$

, where $\vec{u} = (u, v, w)$ are the velocities. Here we have advection components in each of the 3 spatial dimensions, and they can be handled as outlined previously in a dimension by dimension fashion as in [11].

We apply a time splitting as is typical in incompressible flow formulations, first updating the advection terms to obtain an intermediate value of the conserved variables $(\rho)^*$, $(\rho u)^*$, and E^*, and afterward correct these to time t^{n+1} using the pressure. Since the pressure does not affect the continuity equation $\rho^{n+1} = \rho^*$. The non advection momentum and energy updates are

$$\frac{(\rho\vec{u})^{n+1} - (\rho\vec{u})^*}{\Delta t} = -\nabla p \tag{2}$$

and

$$\frac{E^{n+1} - E^*}{\Delta t} = -\nabla \cdot (pu). \tag{3}$$

As in [2], we can use the Euler equations to derive the pressure evolution equation,

$$p_t + \vec{u} \cdot \nabla p = -\rho c^2 \nabla \cdot \vec{u}. \tag{4}$$

Taking motivation from standard incompressible flow solvers, we fix $\nabla \cdot \vec{u}$ to be at time $n + 1$ through the time step, making an $\mathcal{O}(\Delta t)$ error.

$$p_t + \vec{u} \cdot \nabla p = -\rho c^2 \nabla \cdot \vec{u}^{n+1}. \tag{5}$$

Dividing equation (2) by ρ^{n+1}, and noting that $\rho^\star = \rho^{n+1}$, gives

$$\vec{u}^{n+1} = \vec{u}^\star - \Delta t \frac{\nabla p}{\rho^{n+1}} \tag{6}$$

, and following a typical derivation of incompressible flow we take the divergence of equation (6) to obtain

$$\nabla \cdot \vec{u}^{n+1} = \nabla \cdot \vec{u}^\star - \Delta t \nabla \cdot \left(\frac{\nabla p}{\rho^{n+1}} \right) \tag{7}$$

Substituting this into equation (5) gives

$$p_t + \vec{u} \cdot \nabla p = -\rho c^2 \nabla \cdot \vec{u}^\star + \rho c^2 \Delta t \nabla \cdot \left(\frac{\nabla p}{\rho^{n+1}} \right), \tag{8}$$

which is an advection-diffusion equation with source term. Discretizing the $\vec{u} \cdot \nabla p$ advection term explicitly, using a forward Euler time step, and defining the diffusive pressure at time t^{n+1} as is typical for backward Euler discretization, gives after rearrangement

$$p^{n+1} - \rho^n (c^2)^n \Delta t^2 \nabla \cdot \left(\frac{\nabla p^{n+1}}{\rho^{n+1}} \right) = (p^n - (\vec{u}^n \cdot \nabla p^n)\Delta t) - \rho^n (c^2)^n \Delta t \nabla \cdot \vec{u}^\star. \tag{9}$$

Note we have discretized ρc^2 at time t^n. This equation can be further simplified by using the advection equation for pressure,

$$\frac{p^a - p^n}{\Delta t} + \vec{u}^n \cdot \nabla p^n = 0$$

to obtain

$$p^a = p^n - (\vec{u}^n \cdot \nabla p^n)\Delta t,$$

where p^a is an advected pressure which can be computed using HJ ENO [9] or semi-Lagrangian advection [1]. Substituting in equation (9) we obtain

$$p^{n+1} - \rho^n (c^2)^n \Delta t^2 \nabla \cdot \left(\frac{\nabla p^{n+1}}{\rho^{n+1}} \right) = p^a - \rho^n (c^2)^n \Delta t \nabla \cdot \vec{u}^\star. \tag{10}$$

We discretize this equation at cell centers, which is typical for advection-diffusion equations, and thus need to define velocities at cell faces for $\nabla \cdot \vec{u}^\star$. Consider two adjacent grid cells one centered at X_i and one centered at X_{i+1}.

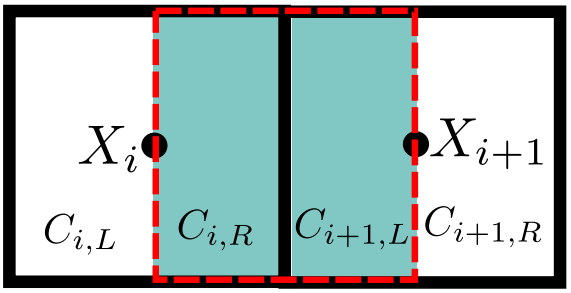

Fig. 1.

We divide these into four regions $C_{i,L}$, $C_{i,R}$, $C_{i+1,L}$, $C_{i+1,R}$, where $(C_{i,R} \cup C_{i+1,L})$ represents a dual cell (see figure 1). Then equation (2) for $C_{i,R}$ is

$$\frac{(\rho u)^{n+1}_{i,R} - (\rho u)^*_{i,R}}{\Delta t} = -\frac{p^{n+1}_{i+1/2} - p^{n+1}_i}{\Delta x/2}. \tag{11}$$

Similarly for $C_{i+1,L}$ we have

$$\frac{(\rho u)^{n+1}_{i+1,L} - (\rho u)^*_{i+1,L}}{\Delta t} = -\frac{p^{n+1}_{i+1} - p^{n+1}_{i+1/2}}{\Delta x/2}. \tag{12}$$

Adding these equations together and dividing by $(\rho_i + \rho_{i+1})$ yields

$$\frac{\hat{u}^{n+1}_{i+1/2} - \hat{u}^*_{i+1/2}}{\Delta t} = -\frac{p^{n+1}_{i+1} - p^{n+1}_i}{\Delta x \hat{\rho}^{n+1}}, \tag{13}$$

where $\hat{u}_{i+1/2} = \frac{(\rho u)_{i,R} + (\rho u)_{i+1,L}}{\rho_i + \rho_{i+1}} = \frac{(\rho u)_i + (\rho u)_{i+1}}{\rho_i + \rho_{i+1}}$ can be thought of as a density-weighted face velocity, and $\hat{\rho}_{i+1/2} = \frac{\rho_i + \rho_{i+1}}{2}$ is the cell face density. Note that

we currently use $(\rho u)_{i,R} = (\rho u)_i$ and $(\rho u)_{i+1,L} = (\rho u)_{i+1}$, although higher order approximations could be used. Using this discretization on equation (10) yields

$$\left[I + \rho^n (c^2)^n \Delta t^2 G^T \left(\frac{1}{\hat{\rho}^{n+1}} G\right)\right] p^{n+1} = p^a + \rho^n (c^2)^n \Delta t G^T \vec{\hat{u}}^\star, \qquad (14)$$

where G is our gradient discretization and $-G^T$ is our divergence discretization and the hat variables are defined as above. This is solved to obtain p^{n+1} at cell centers.

It is interesting to note that this derivation does not require an ideal gas assumption, and hence should be general enough to work with any equation of state (even multi-species flow [2]).

2.2 Updating Momentum and Energy

To obtain the correct shock speeds we need the pressure at cell faces for equations (2) and (3), and the velocity at cell faces for equation (3). Applying conservation of momentum to the control volumes $C_{i,R}$ and $C_{i+1,L}$ (see figure 1) gives

$$Du_{i,R}/Dt = (p_i - p_{i+1/2})/(\Delta x \rho_{i,R}/2)$$

and

$$Du_{i+1,L}/Dt = (p_{i+1/2} - p_{i+1})/(\Delta x \rho_{i+1,L}/2).$$

The constraint that the interface remain in contact implies that $Du_{i,R}/Dt = Du_{i+1,L}/Dt$, which can be used with the aforementioned equations to solve for the pressure at the flux location $X_{i+1/2}$ as

$$p_{i+1/2} = \frac{p_{i+1}\rho_i + p_i \rho_{i+1}}{\rho_{i+1} + \rho_i}. \qquad (15)$$

For solid wall boundaries, we reflect the pressure and density values as usual, and then use equation (15). The cell face velocity is computed via equation (13), and $p_{i+1/2}\hat{u}_{i+1/2}$ is used in equation (3).

3 Time Step Restriction

The eigenvalues of the Jacobian of the advection part of the flux are all u. Since we solve the acoustic component implicitly, we no longer have a severe time step restriction determined by the speed of sound c, and all that remains is to find an estimate for the maximum value of $|u|$ throughout the time step. Simply using u^n is not enough, since e.g. Sod shock tube starts out with an initial velocity identically zero and thus u^n would imply an infinite Δt. To

alleviate this, we add a term that estimates the change in velocity over a time step similar to what was done in [8]. This requires consideration of $\frac{\nabla p}{\rho}$, which we include, in our estimate of the velocity at the end of the time step to get $\left(\frac{|u^n|_{max}+\frac{|p_x|}{\rho}\Delta t}{\Delta x}\right)$ and the CFL condition becomes

$$\Delta t \left(\frac{|u^n|_{max} + \frac{|p_x|}{\rho}\Delta t}{\Delta x}\right) \leq 1 \tag{16}$$

which is quadratic in Δt with solutions

$$\frac{-|u^n|_{max} - \sqrt{|u^n|^2_{max} + 4\frac{|p_x|}{\rho}\Delta x}}{2|p_x|/\rho} \leq \Delta t \leq \frac{-|u^n|_{max} + \sqrt{|u^n|^2_{max} + 4\frac{|p_x|}{\rho}\Delta x}}{2|p_x|/\rho}.$$

As the lower limit is always non positive and $\Delta t \geq 0$, we only need enforce the upper bound. As $p_x \to 0$, both the numerator and denominator vanish and thus we obtain a more convenient time step restriction by replacing the 2^{nd} Δt in equation (16) with this upper bound to obtain

$$\Delta t \left(\frac{|u^n|_{max} + \frac{-|u^n|_{max}+\sqrt{|u^n|^2_{max}+4\frac{|p_x|}{\rho}\Delta x}}{2}}{\Delta x}\right) \leq 1,$$

and our final CFL condition becomes

$$\frac{\Delta t}{2}\left(\frac{|u^n|_{max}}{\Delta x} + \sqrt{\left(\frac{|u^n|_{max}}{\Delta x}\right)^2 + 4\frac{|p_x|}{\rho\Delta x}}\right) \leq 1. \tag{17}$$

Note that this is not linear in Δx, but as $\Delta x \to 0$ we obtain a more typical CFL condition $\Delta t < \frac{\Delta x}{|u^n|_{max}}$.

4 Modified ENO Scheme

When using a traditional ENO methods for the advection part of our equations (as in [11]), we obtained excessive spurious oscillations. This seems to be related to our dual cell center and MAC grid formulation, thus we device a new ENO scheme which better utilizes that dual formulation. We call this Mach-ENO or MENO. The main idea is to replace the advection velocity with the MAC grid value defined at the flux in question, i.e. $\hat{u}$. The lowest level of the divided difference table is typically constructed with the physical fluxes, i.e. ρu, ρu^2 and Eu for $\mathbf{F_1}(\mathbf{U})$ in equation (1). A dissipation term is added for the local and global Lax-Friedrichs versions. Consider constructing

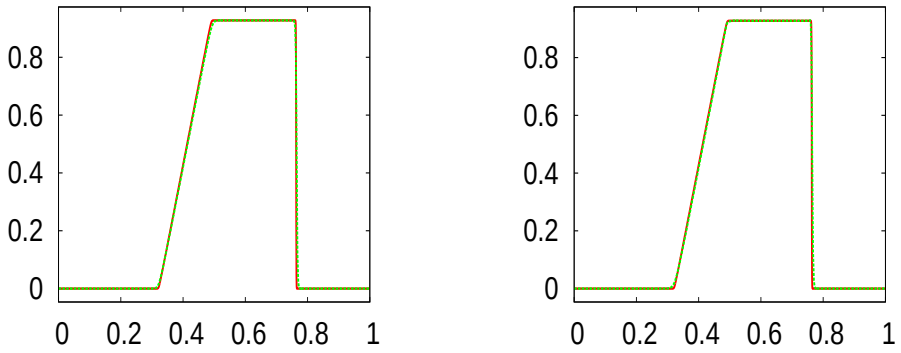

(a) Standard ENO-LLF (b) MENO-LLF

Fig. 2. Sod shock tube problem at $t = .15s$. Left: Standard ENO-LLF using 401 grid points (green) and 1601 grid points (red). Right: The base 1601 grid points solution is the same as in the left figure, but the coarse grid calculation (with 401 grid points) is done with the new MENO scheme. Both simulations were done with explicit time stepping and a full characteristic decomposition in order to demonstrate that the new ENO schemes performs similar to the old one when one is not using our new implicit discretization of the pressure.

an ENO approximation for the flux at $X_{i+1/2}$. Locally, we would use a divided difference table with base values corresponding to the physical fluxes plus or minus the appropriate dissipation. Our modification is to replace $\rho_j u_j$, $\rho_j {u_j}^2$, and $E_j u_j$ with $\rho_j \hat{u}_{i+1/2}$, $\rho_j u_j \hat{u}_{i+1/2}$, and $E_j \hat{u}_{i+1/2}$ leaving the dissipation terms unaltered. Note that $\hat{u}_{i+1/2}$ is fixed throughout the divided difference table similar to the way one fixes the dissipation coefficient.

Figure 2 compares our new MENO scheme to the standard scheme from [11] for standard Sod Shock tube. For this problem the results are fairly similar, but for other test cases the MENO scheme performed much better and in fact the standard ENO scheme was not successful in producing any solution whatsoever for figure 10 in our examples section.

5 Numerical Results

We use third order TVD Runge-Kutta [10] for all our examples. We use two variations of the third order TVD Runge-Kutta scheme in all of our examples. The first is to perform Runge-Kutta on just the advection part, $\mathbf{F_1}(\mathbf{U})$, with only one final implicit solve for $\mathbf{F_2}(\mathbf{U})$. The second variation is to carry out both $\mathbf{F_1}(\mathbf{U})$ and $\mathbf{F_2}(\mathbf{U})$ for each Runge-Kutta stage although this has three times the computational cost as far as the implicit solution of $\mathbf{F_2}(\mathbf{U})$ is con-

cerned. However better numerical results are obtained using the implicit solve within each stage of the Runge-Kutta cycle (see figure 3), and thus that is the scheme employed throughout the rest of the example section, unless otherwise mentioned.

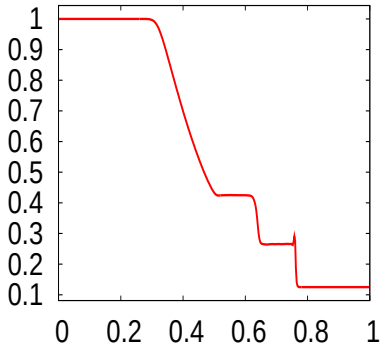

(a) One implicit solve

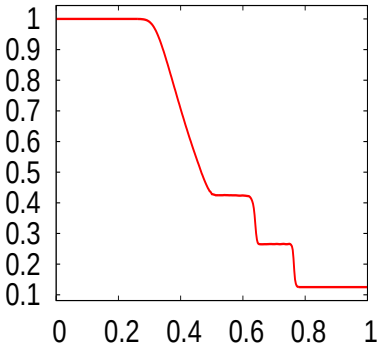

(b) Three implicit solves

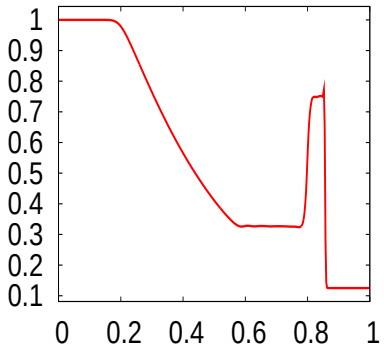

(c) One implicit solve

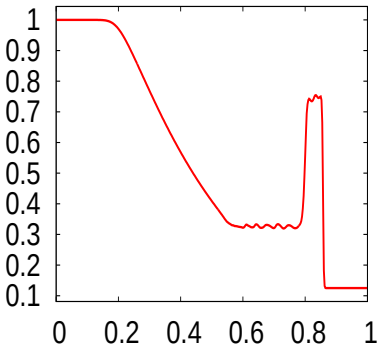

(d) Three implicit solves

Fig. 3. Numerical results comparing placing the implicit solve either inside each Runge-Kutta stage (b and d) or once after a full three stage Runge-Kutta cycle (a and c). The top two figures show the results for a Sod shock tube problem at $t = .15s$, the bottom two figures show the results for a strong shock tube problem at $t = 2.5 \times 10^{-6}s$. Density is shown in all figures. Note the spurious overshoots when the implicit solve is not included in the Runge-Kutta cycle (left two figures).

5.1 One dimensional Validation

For the one dimensional tests, we use a computational domain of $[0, 1]$, 401 grid points, and also plot a baseline solution using 1601 grid points in the standard fully explicit ENO method as in [11]. A second order ENO was used along with the CFL number of .5.

5.1.1 Sod Shock Tube

Our first test case is a standard Sod shock tube with initial conditions of

$$(\rho(x,0), u(x,0), p(x,0)) = \begin{cases} (1,0,1) & \text{if } x \leq .5, \\ (.125,0,.1) & \text{if } x > .5. \end{cases}$$

Our results are shown in Figure 4, which indicate well resolved shock, rarefaction and contact solutions. Since our method is conservative, we get the correct shock speeds.

5.1.2 Lax's Shock Tube

Lax's shock tube is similar in nature to Sod shock tube, except that the initial condition has a discontinuity in the velocity.

$$(\rho(x,0), u(x,0), p(x,0)) = \begin{cases} (.445,.698,3.528) & \text{if } x \leq .5, \\ (.5,0,.571) & \text{if } x > .5. \end{cases}$$

Our results are shown in Figure 5.

5.1.3 Strong Shock Tube

The Strong shock tube problem poses initial conditions that generates a supersonic shock.

$$(\rho(x,0), u(x,0), p(x,0)) = \begin{cases} (1,0,10^{10}) & \text{if } x \leq .5, \\ (.125,0,.1) & \text{if } x > .5. \end{cases}$$

Our results are shown in Figure 6. However the scheme admits some oscillations near the rarefaction wave. Note that the main advantage of the proposed method is to take target time steps irrespective of the sound speed values, one could use the usual ENO scheme for high Mach number flows (or high Mach number regions of the flow – if asynchronous timestepping is used).

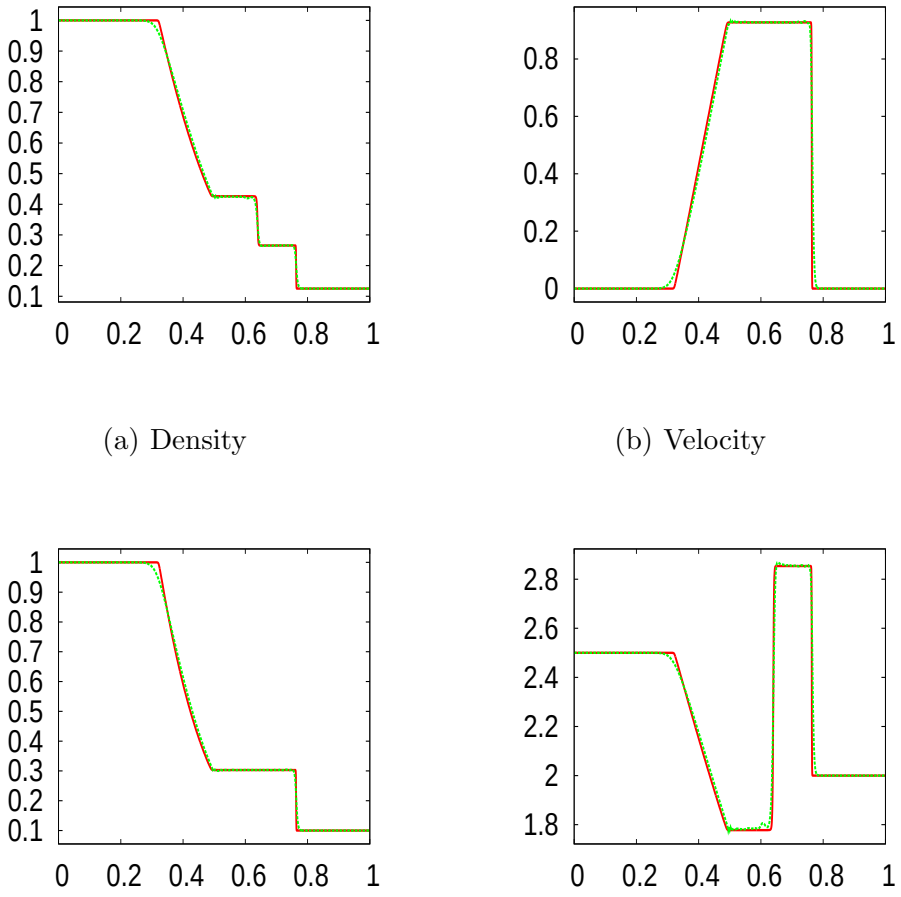

(a) Density

(b) Velocity

(c) Pressure

(d) Internal Energy

Fig. 4. Numerical Results of the Sod shock tube problem at $t = .15s$. The explicit baseline solution is plotted in red, and the solution from our method is plotted in dotted green.

5.1.4 Mach 3 Shock Test

The initial conditions for the Mach 3 shock test are:

$$(\rho(x,0), u(x,0), p(x,0)) = \begin{cases} (3.857, .92, 1.333) & \text{if } x \leq .5, \\ (1, 3.55, 1) & \text{if } x > .5. \end{cases}$$

Our results are shown in Figure 7. As above we do note some oscillations near the rarefaction wave.

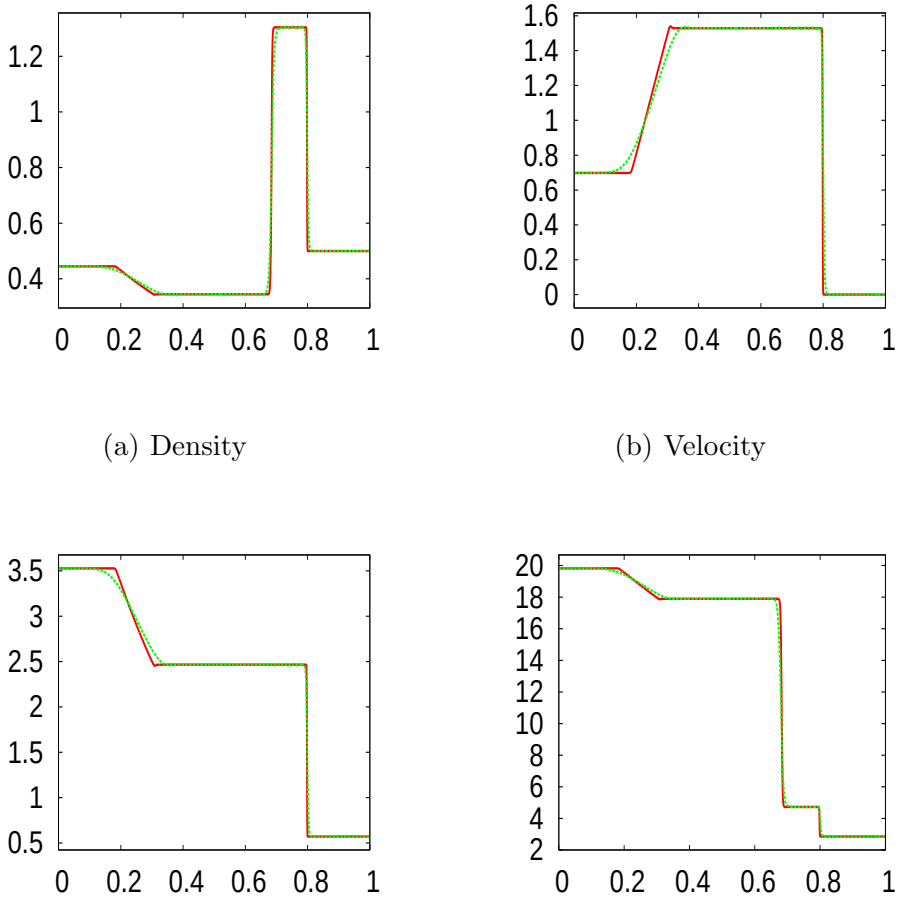

(a) Density

(b) Velocity

(c) Pressure

(d) Internal Energy

Fig. 5. Numerical Results of the Lax's shock tube problem at $t = .12s$. The explicit baseline solution is plotted in red, and the solution from our method is plotted in dotted green.

5.1.5 High mach flow test

The initial conditions for the High mach flow test are:

$$(\rho(x,0), u(x,0), p(x,0)) = \begin{cases} (10, 2000, 500) & \text{if } x \leq .5, \\ (20, 0, 500) & \text{if } x > .5. \end{cases}$$

As noted in [7] the Mach number in this test can reach as high as 240. Our results are shown in Figure 8.

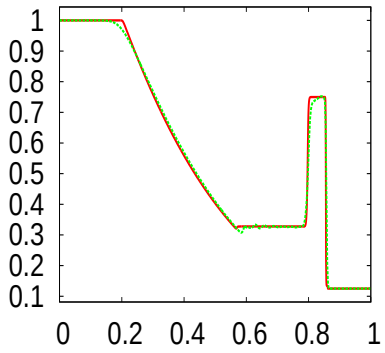

(a) Density

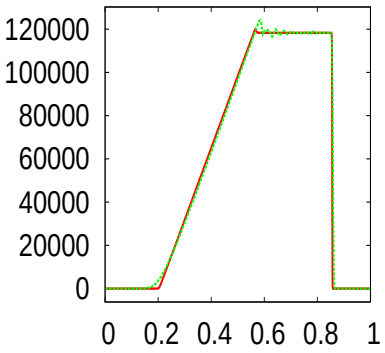

(b) Velocity

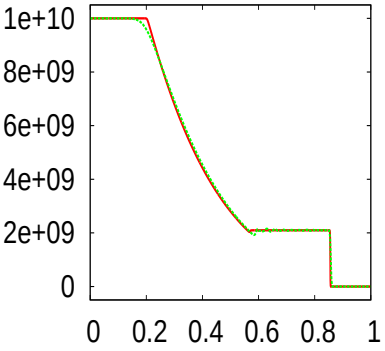

(c) Pressure

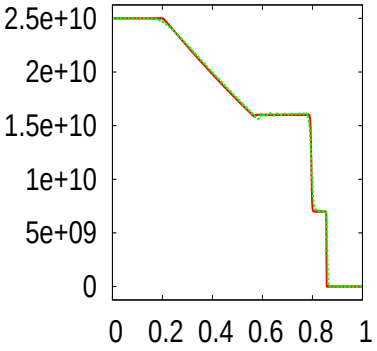

(d) Internal Energy

Fig. 6. Numerical Results of the strong shock tube problem at $t = 2.5 \times 10^{-6}s$. The explicit baseline solution is plotted in red, and the solution from our method is plotted in dotted green.

5.1.6 Interaction of blast waves

Here we present a test of two interacting blast waves. This problem was introduced by [12] and involves multiple strong shock waves. The initial conditions for the test are:

$$(\rho(x,0), u(x,0), p(x,0)) = \begin{cases} (1, 0, 10^3) & \text{if } 0 \leq x < .1, \\ (1, 0, 10^{-2}) & \text{if } .1 \leq x < .9, \\ (1, 0, 10^2) & \text{if } .9 \leq x \leq 1. \end{cases}$$

We also have solid wall boundary conditions at $x = 0$ and $x = 1$. Our results are shown in Figure 9 which shows that we achieve very accurate results.

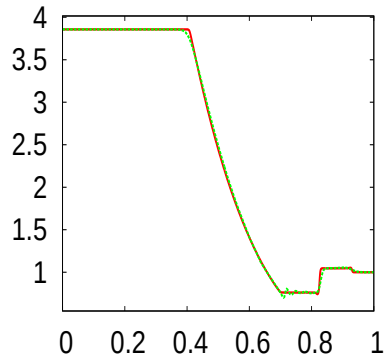

(a) Density

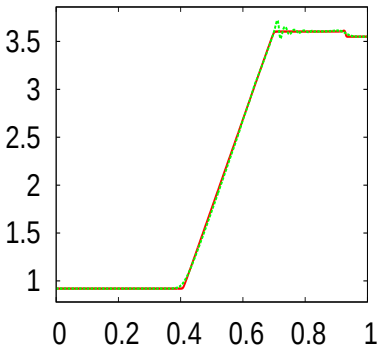

(b) Velocity

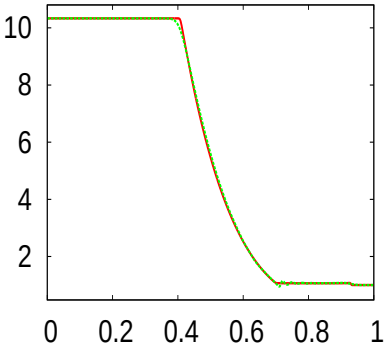

(c) Pressure

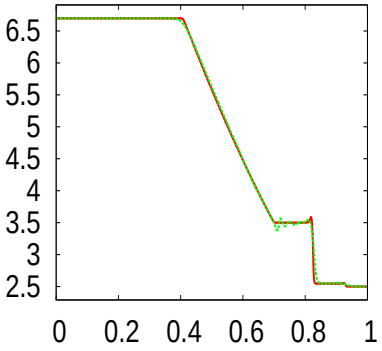

(d) Internal Energy

Fig. 7. Numerical Results of the Mach 3 shock tube problem at $t = .09s$. The explicit baseline solution is plotted in red, and the solution from our method is plotted in dotted green.

5.1.7 Two Symmetric Rarefaction Waves

In this test there are two rarefaction waves going in opposite directions from the center of the domain. This causes very low density regions near the center of the domain. The initial conditions for the test are:

$$(\rho(x,0), u(x,0), p(x,0)) = \begin{cases} (1,-2,.4) & \text{if } x \leq .5, \\ (1,2,.4) & \text{if } x > .5. \end{cases}$$

Our results are shown in Figure 10. Our results are comparable to that of [7] and [13]. Note that there is an unphysical pulse in the internal energy field near the low pressure region, caused by overheating (see e.g. [3]).

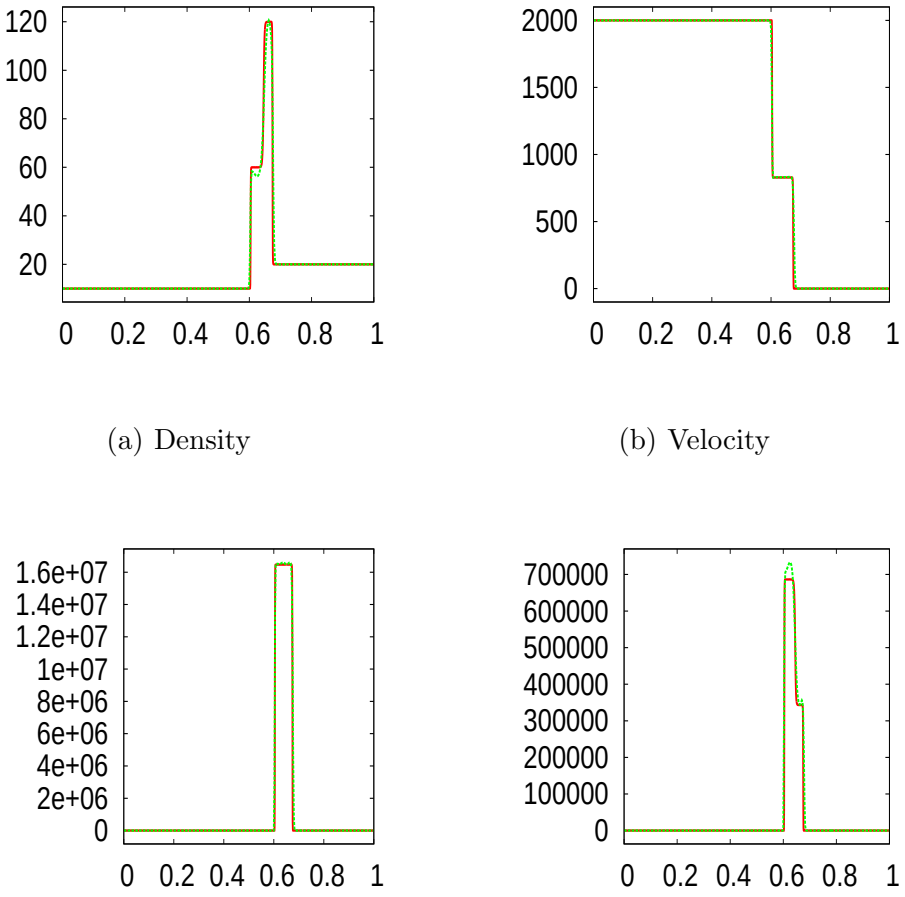

(a) Density (b) Velocity

(c) Pressure (d) Internal Energy

Fig. 8. Numerical Results of the High Mach shock tube problem at $t = 1.75 \times 10^{-4} s$. The explicit baseline solution is plotted in red, and the solution from our method is plotted in dotted green.

5.1.8 Smooth Flow Test (Mach Zero Limit)

The initial conditions for the zero mach limit test are given by:

$$
\begin{aligned}
u(x,0) &= 0 \\
p(x,0) &= p_0 + \epsilon p_1(x) \\
p_1(x) &= 60\cos(2\pi x) + 100\sin(4\pi x) \\
\rho(x,0) &= \left(\frac{p(x,0)}{p_0}\right)^{\frac{1}{\gamma}} \rho_0
\end{aligned}
$$

Where $\rho_0 = 1$, $p_0 = 10^9$, and $\epsilon = 10^3$. Since the flow is smooth and there are no shocks in this test, we have used a single implicit solve per time step. This test is dominated by acoustic waves (as observed in [7]). We can take time

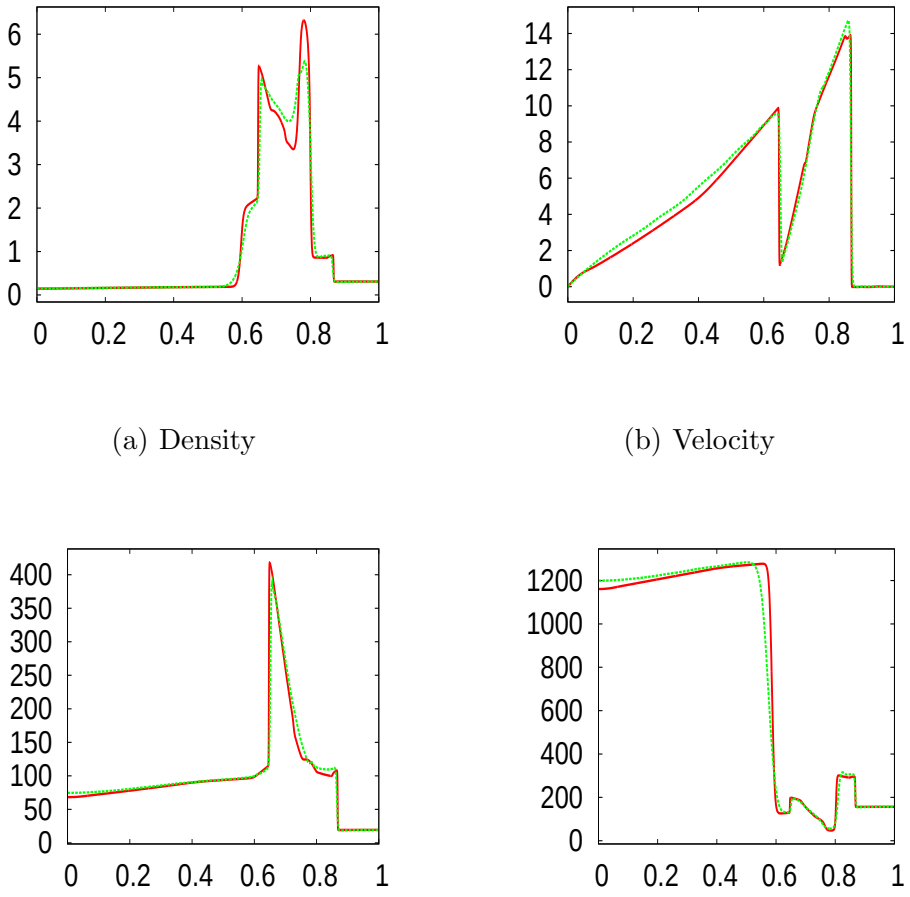

(a) Density

(b) Velocity

(c) Pressure

(d) Internal Energy

Fig. 9. Numerical Results of the interacting blasts shock tube problem at $t = .038s$. The explicit baseline solution is plotted in red, and the solution from our method is plotted in dotted green.

steps as large as is permitted by our CFL condition in equation (17). This permits time steps three orders of magnitude greater than those permitted by sound-speed based CFL. However, as with all implicit schemes, taking too large a time step can lead to inaccurate results. Thus, in order to get sufficient accuracy, we clamp our time step to be a fixed multiple of the explicit time step. In figure 11 we use 3 times the explicit time step and show convergence via grid resolution. In a second suit of tests we show that we can increase the grid resolution without the need for refining the time step. The timing results for this experiment are available in Table 13 where Δt remains fixed as the grid resolution goes up as high as $320,000$ gird cells. At that point the effective sound speed CFL is 300. Numerical results are plotted in figure 12 and Table 13 summarizes the results. In particular whereas the newly proposed implicit method permits a fixed time step all the way up to $320,000$ grid points

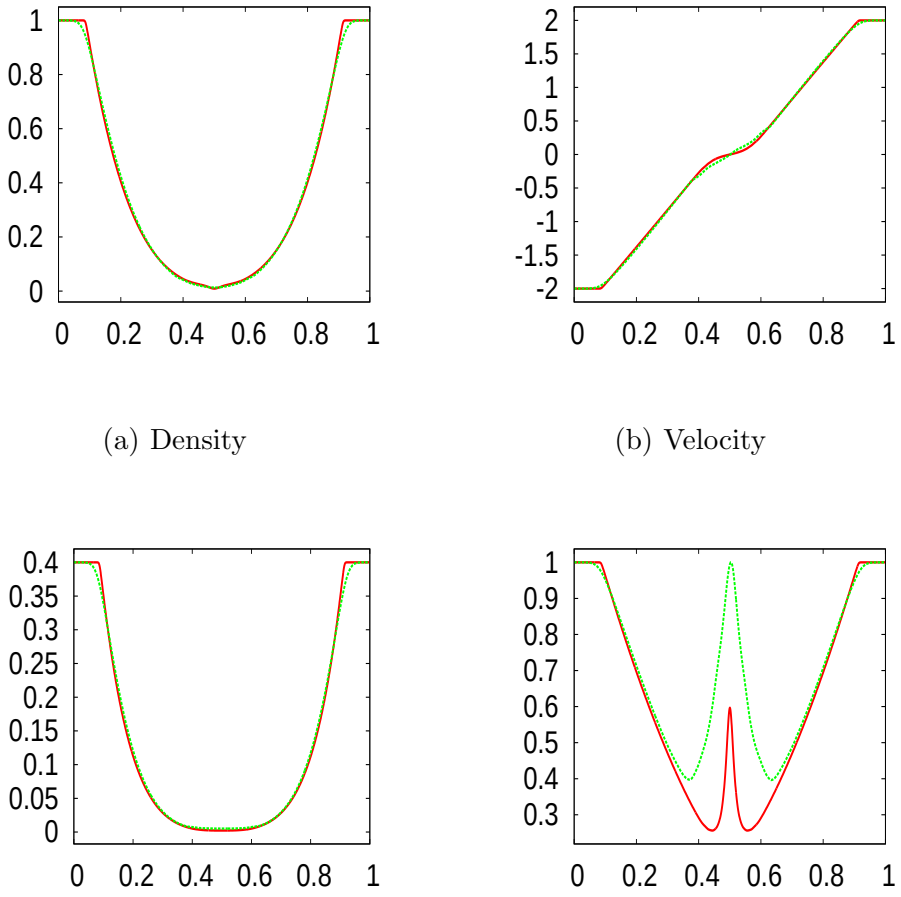

(a) Density

(b) Velocity

(c) Pressure

(d) Internal Energy

Fig. 10. Numerical Results of the symmetric rarefaction shock tube problem at $t = .15s$. The explicit baseline solution is plotted in red, and the solution from our method is plotted in dotted green.

allowing the wall clock simulation time to scale approximately linear to the size of the problem, the explicit simulation time grows quadratically even becoming impractical at $320,000$ grid points.

5.2 Flow Past a Step Test

Our first two dimensional experiment is similar to the one described in [3]. We assume an ideal gas with $\gamma = 1.4$. The test domain is 3 units long and 1 unit wide, with a .2 unit high step which is located .6 units from the left hand side of the tunnel. The initial conditions are $\rho = 1.4$, $p = 1$ and $u = 3$ and $v = 0$ everywhere in the domain. We apply an inflow boundary condition on

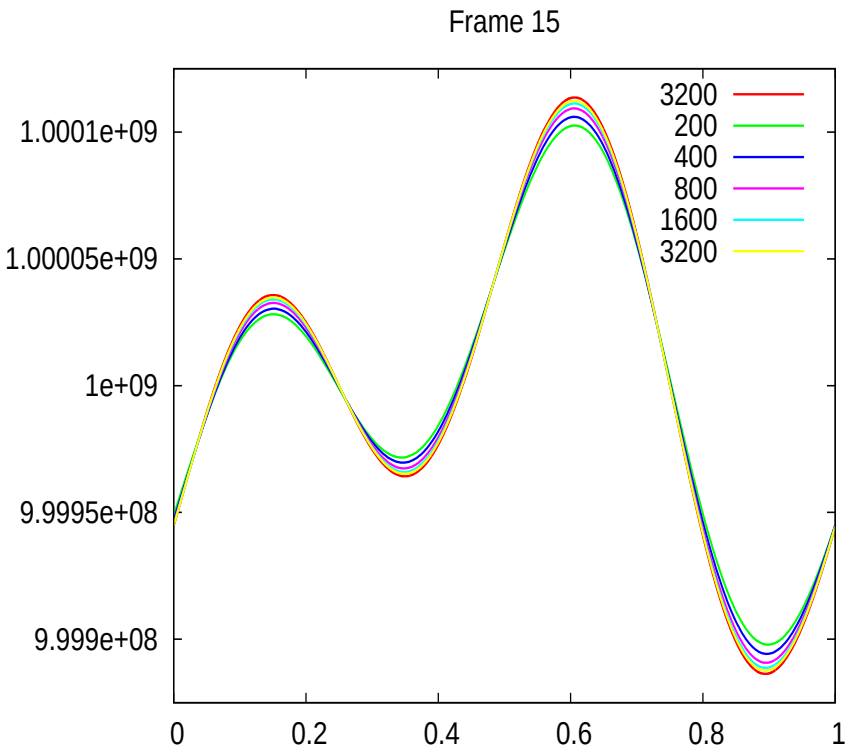

Fig. 11. Numerical results comparing the pressure in smooth flow test at 200, 400, 800, 1600, and 3200 grid cells with an effective sound speed based CFL number 3 at $t = 1.5 \times 10^{-5} s$. The red curve is the explicit simulation run at 3200 grid cells with a CFL number .5.

the left hand side of the domain, and an outflow boundary condition on the right hand side of the domain. A reflective solid wall boundary condition is applied for the top and bottom boundaries of the domain. We show numerical results at $t = 4s$ on a grid of resolution 120x40 in figure 14.

5.3 Circular Shock Test

The circular shock test has an initial condition prescribed as

$$(\rho, u, v, p) = \begin{cases} (1, 0, 0, 1) & \text{if } r \leq .4 \\ (.125, 0, 0, .1) & \text{if } r > .4 \end{cases}$$

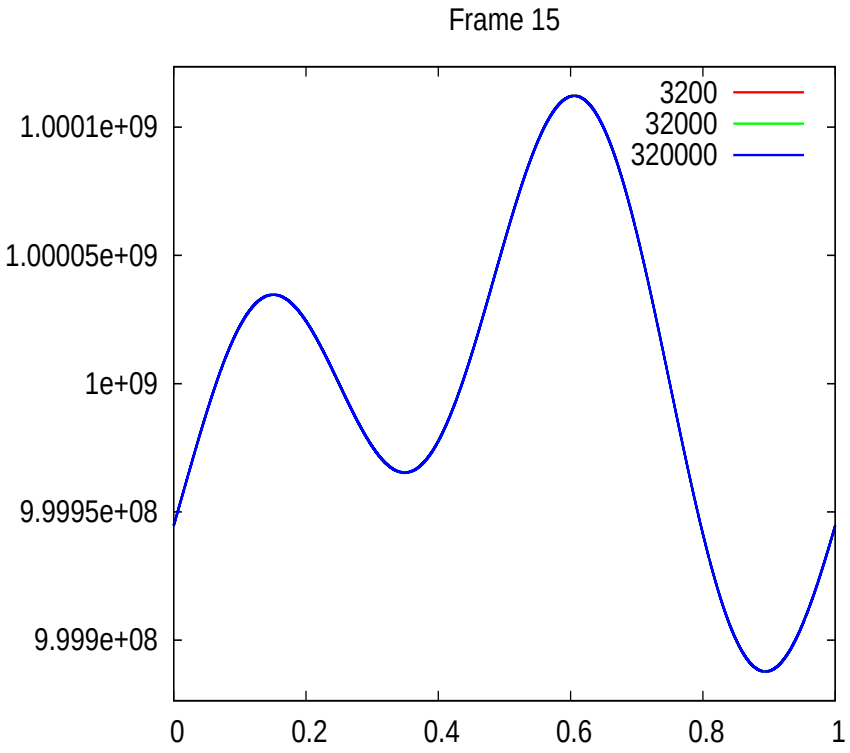

Fig. 12. Numerical results showing pressure in smooth flow test at 3200, 32000 and 320000 grid cells. We used an effective sound speed based CFL number of 3, 30 and 300 respectively at $t = 1.5 \times 10^{-5}s$. Since Δt stays constant, the solution remains relatively unchanged even as we get huge time step gains.

Grid Resolution	Effective sound speed CFL	Δt	Wall clock time (Implicit)	Wall clock time (Explicit)
3200	3	5.01e-08	63.41s	511.67s
32000	30	5.01-08	810.03s	60498.49s
320000	300	5.01e-08	9976.58s	Impractical

Fig. 13. Timing results for smooth flow test, with Δt approximately constant. The wall clock times are shown for simulations till $t = 5 \times 10^{-5}s$.

where $r = \sqrt{x^2 + y^2}$. Numerical results are shown in figure 15. The same test was shown in [14]. Our results indicate well resolved shock and contact solutions along with correct speed shock calculations.

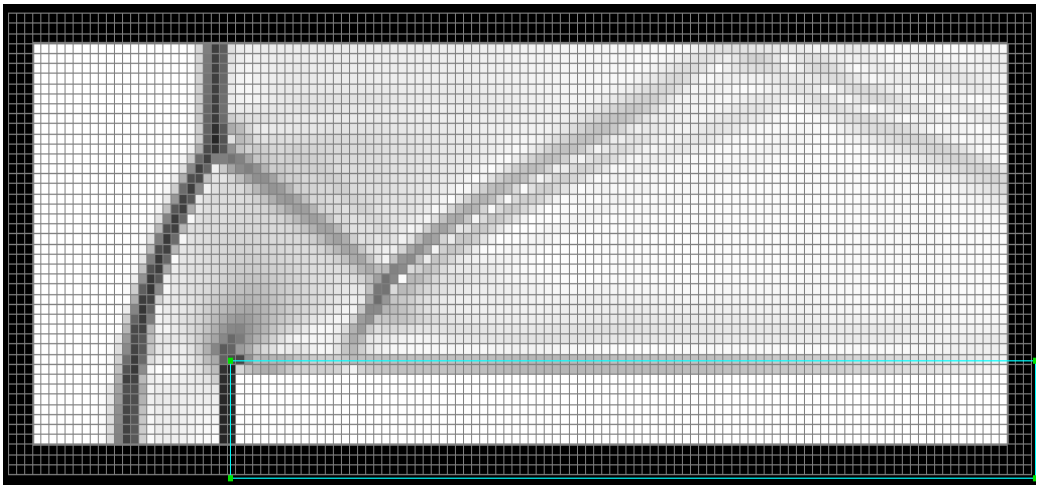

Fig. 14. Numerical results showing the Schlerian plots of density for the flow past a step test on a grid of size 120x40 at $t = 4s$.

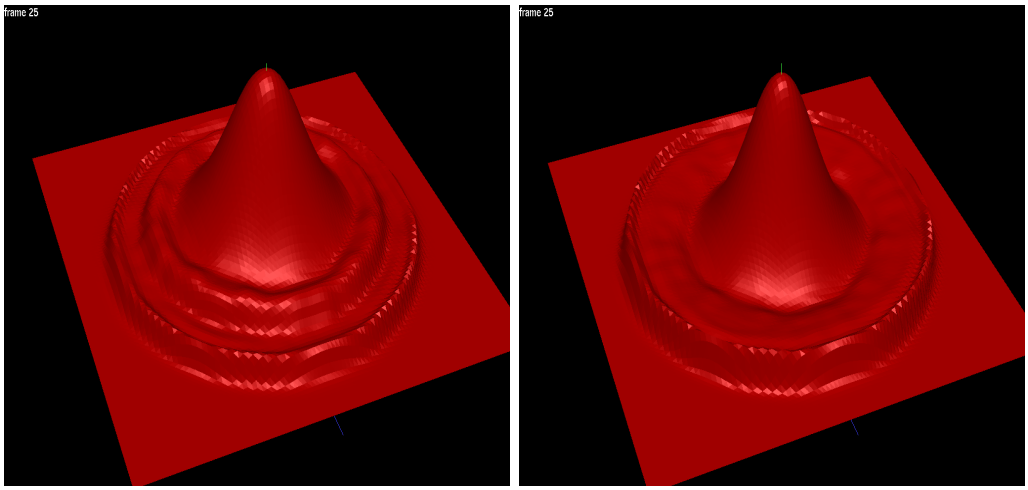

(a) Density (b) Pressure

Fig. 15. Numerical results for the circular shock test on a grid of size 100x100 at $t = .25s$.

6 Conclusions and Future Work

We have presented a method for alleviating the stringent CFL condition imposed by the sound speed in highly non-linear compressible flow simulations. A fractional step procedure combined with the pressure evolution equation is used. The method works for arbitrary equations of state; and in the limit as the sound speed goes to infinity, it yields the Poisson equation for incompressible flow. We also presented a Mach-ENO or MENO scheme which better utilizes a dual cell center and MAC grid formulation. The numerical experiments on various benchmark problems for one and two dimensions indicate that our semi-implicit method obtains well resolved shock, rarefaction and

contact solutions. Since our method is conservative, we also obtain correct shock speeds. The smooth flow example illustrates the ability of our method to take significantly large time steps for low Mach number flows as compared to explicit methods. In future work we plan to extend our approach to handle two-way coupling between compressible and incompressible flows, as well as fully implicit solid-fluid coupling.

7 Acknowledgments

Research supported in part by a Packard Foundation Fellowship, an Okawa Foundation Research Grant, ONR N0014-06-1-0393, ONR N00014-06-1-0505, ONR N00014-02-1-0720, ONR N00014-05-1-0479 for a computing cluster, NIH U54-GM072970, NSF ACI-0323866, NSF IIS-0326388, NSF ITR-0205671 and NSF CCF-0541148. J.S. was supported in part by an NSF Graduate Research Fellowship.

A Boundary Conditions

Figure 14 requires the handling of inflow and outflow boundary conditions. We define U_{out} to be the outgoing state and U_{in} to be the ingoing state. The outgoing state, U_{out}, is obtained by simple extrapolation whereas the ingoing state, U_{in}, is obtained by attenuating U_{out} towards specified far-field values. After defining U_{out} via extrapolation, we average the primitive variables to cell flux on the boundary of the domain, and use those values to compute a characteristic decomposition. If the p^{th} characteristic field indicates ingoing information, then when applying the ENO scheme in this characteristic field we use U_{in} for the ghost node values. Otherwise U_{out} is used. Note for higher order schemes boundary values will be needed for fluxes on the interior of the domain as well, and we choose the ghost nodes (as U_{in} or U_{out}) in the same fashion.

Our ingoing state, U_{in}, is calculated as follows. Our ingoing state, U_{in}, is obtained by attenuating the extrapolated state, U_{out}, towards a given far field state, U_{far}. This is accomplished by multiplying U_{out} with each of the left eigenvectors, attenuating if the eigenvalue in that characteristic field indicates an ingoing wave, and then multiplying by the right eigenvector. Defining the scalar characteristic information in each field as $\xi^p = L^p U_{out}$, we would attenuate ξ^p towards ξ^p_{far} using the analytic solution of the ODE

$$d\xi/dt = K(\xi - \xi_{far})$$

for time step Δt using initial data of $\xi = \xi_{out}$. We used an attenuation coefficient of $K = -.5$ in our examples.

References

[1] R. Courant, E. Issacson, and M. Rees. On the solution of nonlinear hyperbolic differential equations by finite differences. *Comm. Pure and Applied Math*, 5:243–255, 1952.

[2] R. Fedkiw, X.-D. Liu, and S. Osher. A general technique for eliminating spurious oscillations in conservative schemes for multiphase and multispecies euler equations. *Int. J. Nonlinear Sci. and Numer. Sim.*, 3:99–106, 2002.

[3] R. Fedkiw, A. Marquina, and B. Merriman. An isobaric fix for the overheating problem in multimaterial compressible flows. *J. Comput. Phys.*, 148:545–578, 1999.

[4] R. Fedkiw, B. Merriman, and S. Osher. Efficient characteristic projection in upwind difference schemes for hyperbolic systems (the complementary projection method). *J. Comput. Phys.*, 141:22–36, 1998.

[5] G.-S. Jiang and C.-W. Shu. Efficient implementation of weighted ENO schemes. *J. Comput. Phys.*, 126:202–228, 1996.

[6] S.Y. Kadioglu and M. Sussman. Adaptive solution techniques for simulating underwater explosions and implosions. *J. Comput. Phys.*, 227:2083–2104, 2008.

[7] S.Y. Kadioglu, M. Sussman, S. Osher, J. Wright, and M. Kang. A second order primitive preconditioner for solving all speed multi-phase flows. *J. Comput. Phys.*, 209:477–503, 2005.

[8] M. Kang, R. Fedkiw, and X.-D. Liu. A boundary condition capturing method for multiphase incompressible flow. *J. Sci. Comput.*, 15:323–360, 2000.

[9] S. Osher and C.-W. Shu. High order essentially non-oscillatory schemes for Hamilton-Jacobi equations. *SIAM J. Num. Anal.*, 28:902–921, 1991.

[10] C.-W. Shu and S. Osher. Efficient implementation of essentially non-oscillatory shock capturing schemes. *J. Comput. Phys.*, 77:439–471, 1988.

[11] C.-W. Shu and S. Osher. Efficient implementation of essentially non-oscillatory shock capturing schemes II (two). *J. Comput. Phys.*, 83:32–78, 1989.

[12] P. Woodward and P. Colella. The numerical simulation of two-dimensional fluid flow with strong shocks. *Journal of Computational Physics*, 54:115–173, April 1984.

[13] F. Xiao. Unified formulation for compressible and incompressible flows by using multi-integrated moments I: one-dimensional inviscid compressible flow. *J. Comput. Phys.*, 195:629–5654, 2004.

[14] F. Xiao, R. Akoh, and S. Ii. Unified formulation for compressible and incompressible flows by using multi-integrated moments II: Multi-dimensional version for compressible and incompressible flows. *J. Comput. Phys.*, 213:31–56, 2006.

[15] T. Yabe and P.Y. Wang. Unified numerical procedure for compressible and incompressible fluid. *Journal of the Physical Society of Japan*, 60:2105–2108, July 1991.

[16] S.Y. Yoon and T. Yabe. The unified simulation for incompressible and compressible flow by the predictor-corrector scheme based on the CIP method. *Comput. Phys. Commun.*, 119:149–158, 1999.